Time-Domain Electron Paramagnetic Resonance as a Probe of Electron–Electron Spin–Spin Interaction in Spin-Labeled Low-Spin Iron Porphyrins

Margaret H. Rakowsky, Kundalika M. More, Alexander V. Kulikov, Gareth R. Eaton, and Sandra S. Eaton*

Contribution from the Department of Chemistry, University of Denver, Denver, Colorado 80208

Received February 7, 1994[⊗]

Abstract: Nitroxyl free radical electron spin relaxation times for spin-labeled complexes of low-spin iron(III) porphyrins were measured between 8 and 70 K by two-pulse spin-echo spectroscopy and between 8 and 120 K by saturation recovery. Relaxation times for low-spin Fe^{III}(TPP)(MeIm)$_2$ (TPP = tetraphenylporphyrin; MeIm = methylimidazole) were measured between 10 and 28 K by saturation recovery and between 10 and 25 K by electron spin-echo. At low temperature the iron electron spin relaxation rates are slow relative to the electron–electron spin–spin splitting. As temperature is increased, the relaxation rates for the Fe(III) become comparable to and then greater than the spin–spin splitting, which collapses the splitting in the continuous wave EPR spectra and causes an increase and then a decrease in the nitroxyl spin-echo decay rate. Throughout the temperature range examined, interaction with the Fe(III) increases the spin-lattice relaxation rate ($1/T_1$) for the nitroxyl. The measured relaxation times for the Fe(III) were used to analyze the temperature-dependent changes in the spin-echo decays and in the saturation recovery (T_1) data for the interacting nitroxyl and determine the interspin distance, r. The values of r for the four complexes that were examined were between 10.5 and 15 Å, with good agreement between values obtained by spin-echo and saturation recovery. For each of the compounds the value of r is consistent with other data for that spin-labeled porphyrin. Analysis of the nitroxyl spin-echo and saturation recovery data also provide values of the iron relaxation rates at temperatures where the rates are too fast to measure directly by saturation recovery or electron spin-echo spectroscopy. These data demonstrate the power of time-domain EPR measurements as a probe of distance between a slowly-relaxing spin and a relatively rapidly relaxing metal ion such as low-spin Fe(III).

Introduction

Electronic spectra and magnetic properties of iron are sensitive reporters of the iron environment. The wide range of oxidation states, spin states, and geometries already observed for iron in biological systems necessitates probing the iron with the most sensitive techniques available.[1] Various double-probe methods have proven valuable in many aspects of biochemistry. One example is the use of two paramagnetic species, which permits study of their interactions with each other in addition to their interaction with other aspects of their environment.[2] The CW EPR (continuous wave electron paramagnetic resonance) of a nitroxyl spin label in the presence of a paramagnetic iron center reports on the relaxation time of the iron.[3] Since the CW EPR of both the iron and the nitroxyl radical are broadened by unresolved hyperfine interactions and by g and a anisotropies, changes in electron spin relaxation times are reported more sensitively by time domain EPR than by CW EPR. With the increasing availability of pulsed, time-domain EPR, new vistas on electron spins are being revealed.[4,5] In this paper we demonstrate the detailed information that is revealed by electron spin-echo (ESE) and saturation recovery (SR) EPR of low-spin Fe(III) interacting with a nitroxyl spin label. The approaches are general and could be applied to many interacting spin systems, elucidating both the properties of the fast relaxing center and the interaction between the two centers.

When there is electron–electron spin–spin coupling between two paramagnetic centers, AB splitting patterns can be observed in the CW EPR spectra provided that the relaxation rates in hertz ($1/T_1$ and $1/T_2$) for the faster-relaxing center are slow compared with the magnitude of the spin–spin splitting expressed in hertz.[6,7] As the relaxation rates increase and become comparable to the spin–spin splitting, the lines of the AB pattern broaden and coalesce. As the electron spin relaxation rates increase further, the lines sharpen to an average position, analogous to the averaging that occurs as a function of temperature in a dynamic NMR experiment.[8] Observations of the collapse of electron–electron spin–spin splitting with increasing temperature have been reported in the literature. For example, in the EPR spectra of spin-labeled high-spin iron(III) porphyrins resolved splitting of the Fe(III) and nitroxyl signals is observed at 8 K, but increasing rates of relaxation of the Fe(III) unpaired electron spin result in collapse of the splitting at higher temperatures.[9] In a second example, spin–spin splitting of the EPR spectrum of the Ni(I) center in hydrogenase from *C. vinosum* is resolved at 4.2 K, but it is fully averaged when the temperature is increased to 25 K due to increasing rates of relaxation of the iron–sulfur cluster to which the Ni(I) center is coupled.[10] For complexes with these magnitudes of spin–

[⊗] Abstract published in *Advance ACS Abstracts*, February 1, 1995.

(1) Smith, T. D.; Pilbrow, J. R. *Biol. Magn. Reson.* **1980**, *2*, 85.
(2) Hyde, J. S.; Swartz, H. M.; Antholine, W. E. *Spin Labeling* **1979**, *2*, 71.
(3) More, K. M.; Eaton, G. R.; Eaton, S. S. *Inorg. Chem.* **1985**, *24*, 3820.
(4) Hoff, A. J., Ed. *Advanced EPR: Applications in Biology and Biochemistry*; Elsevier: Amsterdam, 1989.
(5) Kevan, L.; Bowman, M. K., Eds. *Modern Pulsed and Continuous-Wave Electron Spin Resonance*; Wiley: New York, 1990.
(6) Eaton, G. R.; Eaton, S. S. *Acc. Chem. Res.* **1988**, *21*, 107.
(7) Eaton, G. R.; Eaton, S. S. *Biol. Magn. Reson.* **1989**, *8*, 339.
(8) Drago, R. S. *Physical Methods for Chemists*, 2nd ed.; Saunders College Publishing: Fort Worth, 1992; Chapter 8.
(9) Fielding, L.; More, K. M.; Eaton, G. R.; Eaton, S. S. *J. Am. Chem. Soc.* **1986**, *108*, 8194.
(10) van der Zwaan, J. W.; Albracht, S. P. J.; Fontijn, R. D.; Mul, P. *Eur. J. Biochem.* **1987**, *169*, 377.

0002-7863/95/1517-2049$09.00/0

Chart 1

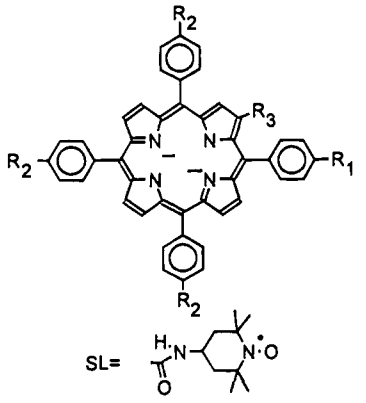

R_1	R_2	R_3	
SL	CH_3	H	p-TTP-SL
H	H	*cis* -CH=CH-SL	*cis*-TPP-SL
H	H	*trans* -CH=CH-SL	*trans*-TPP-SL
H	H	$-CH_2-CH_2-SL$	*satd*-TPP-SL
H	H	H	TPP

spin interaction, the splittings are well-resolved at low temperature and the line shape changes with temperature are readily observed. However, for weaker spin−spin interactions the spin−spin splittings are smaller and the line shape changes with temperature due to collapse of the splittings are more subtle. It would be helpful to have a method other than line shape changes to analyze the spin−spin interaction.

The effects on CW EPR spectra of the dynamic averaging of electron−nuclear spin−spin splittings by methyl group rotation have been observed.[11] In the temperature range where methyl group rotation is slow relative to electron−nuclear couplings, the unpaired electron is coupled to three inequivalent protons. As the rate of methyl group rotation increases, the three protons become equivalently coupled to the unpaired electron on the experimental timescale. ESE measurements have been used to monitor this dynamic averaging process even when the splitting that is averaged is small relative to overall line width.[12−15] In the regime of intermediate rates of rotation, the averaging of inequivalent environments results in increased rates of ESE decay that have been observed for nitroxyl radicals,[12−14] Cr(V) complexes,[14] and copper complexes including Cu^{II}(diethyldithiocarbamate)$_2$.[15] The effect of dynamic processes on ESE decay for acetate anion also has been examined.[16]

Increasing rates of electron spin−lattice relaxation for the faster relaxing partner of an electron−electron spin−spin coupled system as temperature is increased is a dynamic process analogous to a physical motion such as methyl rotation that averages inequivalent sites. Thus it should be possible to monitor the collapse of this spin−spin splitting as a function of temperature via changes in ESE decay rates for the slower relaxing partner. These changes are likely to be more sensitive than overall line shape to collapse of small splittings. In this paper this effect is demonstrated in ESE studies as a function of temperature from 8 to 70 K for four porphyrin complexes in which low-spin Fe(III) is spin-coupled to a nitroxyl radical. The structural formulas for the complexes are shown in Chart 1.

Although it has been recognized for many years that interaction of a slower relaxing paramagnetic center with a faster relaxing center causes an increase in the relaxation rate of the slower relaxing center,[7] we are not aware of any case in which measured rates of relaxation for the faster relaxing center have been used to quantitatively interpret its effect on the relaxation rate of the slower relaxing center. In this report we show that the effect of the low-spin Fe(III) on T_1 for an interacting nitroxyl radical can be interpreted quantitatively to obtain the interspin distance. The interspin distance and iron relaxation rates obtained by analysis of the nitroxyl ESE and SR data are consistent.

Experimental Section

Preparation of Compounds. 5,10,15,20-Tetraphenylporphyin (H_2-TPP),[17] Fe(TPP)Cl,[18] and 5-(4-carboxyphenyl)-10,15,20-tritolylporphyrin (H_2-*p*-COOH-TTP)[19] were prepared by literature methods. Fe(*cis*-TPP-SL)Cl, Fe(*trans*-TPP-SL)Cl, and precursors were prepared by literature methods[20,21] with some modifications. The acrylate ester porphyrins were prepared as the copper complexes by Momenteau's method I.[22] The cis and trans esters were separated by chromatography in toluene on silica gel. An aquarium pump was used to apply a positive pressure to the top of the column to accelerate the rate of flow of solvent through the column. The porphyrins were demetalated by dropwise addition of H_2O to a solution containing $POCl_3$.[23] Insertion of Fe(II), which air oxidizes to Fe(III), was performed by the method of Adler.[18] Formation of the acid chloride and attachment of the spin label[21] were done in rigorously dried glassware and solvents under a nitrogen atmosphere. The product isolated after chromatography typically is a mixture of oxo dimer and axial chloride complexes. After conversion to the axial chloride, visible spectra were in good agreement with data for previous samples for which elemental analyses had been obtained.[21]

Fe(*satd*-TPP-SL)Cl was prepared by procedures similar to that for the cis and trans isomers except that demetalated porphyrin (either the cis or trans isomer) was hydrogenated by the method of Momenteau.[22] The product was characterized by visible spectroscopy and quantitation of the nitroxyl EPR signal.[21]

Fe(*p*-TTP-SL)Cl was prepared from (H_2-*p*-COOH-TTP) by procedures analogous to those used to prepare the cis, trans, and saturated spin-labeled porphyrins.[21] Yield for conversion of Fe(*p*-COOH-TTP)-Cl to Fe(*p*-TTP-SL)Cl: 89%. IR: $\nu_{CO} = 1665\ cm^{-1}$. Visible spectrum ($CHCl_3$ solution, wavelengths in nm and log(ϵ) in parentheses): 421 (5.09), 510 (4.15), 575 (3.52), 697 (3.51). EPR spectra in fluid solution: integrated intensity of nitroxyl signal relative to a standard

(11) Gamble, W. L.; Miyagawa, I.; Hartman, R. L. *Phys. Rev. Lett.* **1968**, *20*, 415.
(12) Dzuba, S. A.; Salikhov, K. M.; Tsvetkov, Yu. D. *Chem. Phys. Lett.* **1981**, *79*, 568.
(13) Tsvetkov, Yu. D.; Dzuba, S. A. *Appl. Magn. Reson.* **1990**, *1*, 179.
(14) Nakagawa, K.; Candelaria, M. B.; Chik, W. W. C.; Eaton, S. S.; Eaton, G. R. *J. Magn. Reson.* **1992**, *98*, 81.
(15) Du, J.-L.; Eaton, G. R.; Eaton, S. S. *Appl. Magn. Reson.* **1994**, *6*, 373.
(16) Kispert, L. D.; Bowman, M. K.; Norris, J. R.; Brown, M. S. *J. Chem. Phys.* **1982**, *76*, 26.
(17) Adler, A. D.; Longo, F. R.; Finarelli, J. D.; Goldmacher, J.; Assour, J.; Korsakoff, L. *J. Org. Chem.* **1967**, *32*, 476.
(18) Adler, A. D.; Longo, F. R.; Kampas, F.; Kim, J. *J. Inorg. Nucl. Chem.* **1970**, *32*, 2443.
(19) Anton, J. A.; Kwong, J.; Loach, P. A. *J. Heterocycl. Chem.* **1976**, *13*, 717.
(20) More, K. M.; Eaton, S. S.; Eaton, G. R. *Inorg. Chem.* **1981**, *20*, 2641.
(21) More, K. M.; Eaton, G. R.; Eaton, S. S. *J. Magn. Reson.* **1984**, *60*, 54.
(22) Momenteau, M.; Loock, B.; Bisagni, E.; Rougee, M. *Can. J. Chem.* **1979**, *57*, 1804.
(23) Ponomarev, G. V.; Maravin, G. B. *Khim. Geterotsikl. Soedin.* **1977**, *86*, 72 in translation.

sample indicated 100% spin label attachment. EPR spectra in frozen solution showed a 1:1 ratio of high-spin iron(III) to nitroxyl radical.

Preparation of Solutions for EPR Studies. As isolated, solid samples of the iron porphyrin chlorides typically contained some oxo-bridged dimer. The following procedure was used to convert oxo dimer to monomer. To prepare a solution with a final concentration of 1 mM in 2:1 toluene−$CHCl_3$ containing 10% MeIm (1-methylimidazole), 1.5 μmol of iron(III) porphyrin chloride was dissolved in 1.0 mL of toluene in a 2.0 mL volumetric flask. KOH or NaOH (1.0 mL, 0.05 M) was added and the mixture was shaken vigorously for several minutes. The aqueous layer was removed carefully. This procedure was repeated a second and sometimes a third time (if visible spectra indicated incomplete conversion) to convert the complex completely to the hydroxide form. HCl (1.0 mL, 2%) was added and the mixture was shaken vigorously for 5 min. After removal of the aqueous layer, 0.5 mL of $CHCl_3$ was added. The organic solution was transferred to a 5 mL beaker, swirled to allow any remaining water droplets to adhere to the beaker, and transferred to a clean, dry volumetric flask. MeIm (0.15 mL) was added to convert the high-spin chloride complex to low-spin Fe(porphyrin-SL)$(MeIm)_2^+$. An aliquot of the solution was transferred to a 4 mm o.d. quartz EPR tube, degassed by a minimum of 3 freeze−pump−thaw cycles, and the tube was back-filled with a partial pressure of N_2. The remainder of the solution could be stored at 0 °C for up to 2 weeks without degradation.

Saturation Recovery Measurements. A locally-contructed spectrometer[24] was used for the SR measurements. Temperatures between 5 and 70 K were obtained with liquid helium and an Oxford ER900 flow cryostat. Temperatures between 80 and 120 K were obtained with liquid nitrogen and a Varian dewar flow assembly. To test for spectral diffusion the pump time was increased until further increase gave no detectable change in the recovery time constant. Pump times used for data collection were $>T_1$. Typically 5000 to 10000 recovery curves were signal averaged in a LeCroy digital oscilloscope and transferred to a PC for data analysis. Data were fit to a single exponential with locally-written software.

Electron Spin-Echo Measurements. ESE decays were recorded on a locally constructed spectrometer operating at ca. 9.2 GHz with an over-coupled Varian V4531 TE_{102} resonator.[25] A $90-\tau-180-\tau-$echo sequence was used. The time for a 90° pulse was 20 ns. Typically echo decays of 512 data points were recorded starting at 200 ns and extended for 2 to 15 μs. Temperatures between 5 and 70 K were obtained with an Oxford ER900 flow cryostat. For both the SR and ESE systems temperatures were calibrated by replacing the sample-containing tube with a tube containing a thermocouple immersed in 1:1 water−glycerol. The uncertainty in temperature is estimated to be ±1 K. CW spectra were recorded in the continuous wave mode of the ESE spectrometer.[25]

The time constant for the ESE decay is referred to as T_m to encompass all processes that result in echo dephasing (see discussion below). The values obtained directly from experiment are typically cited as decay time constants. In the ensuing discussion it is often more direct to refer to relaxation rates, which are the reciprocals of the time constants.

For 1 mM frozen solutions of nitroxyl radicals at the temperatures and pulse lengths examined in these studies, T_m is weakly dependent upon B_1, which indicates that instantaneous diffusion[26] due to spin flips of a neighboring radical during the second microwave pulse makes a minor contribution to T_m. To the extent that this process contributes to T_m, it will be about the same for H_2(*trans*-TPP-SL) and for the spin-labeled iron complexes and does not contribute to differences between them. (The low-spin Fe(III) EPR signal extends over about 2000 G so the probability that a neighboring Fe(III) is flipped by the second microwave pulse and thereby changes the resonance of the interacting nitroxyl is negligibly small.) For $FeTPP(MeIm)_2^+$ the value of T_m was independent of microwave B_1 which indicates that instantaneous diffusion makes a negligible contribution to the dephasing process.[26] There was no indication of dynamic processes contributing to T_m so T_m is a reasonable estimate of T_2.

Analysis of Experimental Data

Analysis of CW Spectra. CW spectra of H_2(*trans*-TPP-SL) and Fe(TPP)$(MeIm)_2^+$ at 100 K were analyzed with the locally written program MONMER, which uses perturbation calculations, assumes that the principal axes of the **g** and **A** matrices are collinear, and treats hyperfine interactions to second order.[27] Nitroxyl parameters are $g_x = 2.0095$, $g_y = 2.0053$, $g_z = 2.0025$, $A_x = 4 \times 10^{-4}$, $A_y = 6 \times 10^{-4}$, $A_z = 33.5 \times 10^{-4}$ cm^{-1}. The relative values of the g components are more precise than the absolute values due to uncertainties in the external field calibration. The parameters for low-spin Fe(TPP)$(MeIm)_2^+$ are $g_x = 1.500$, $g_y = 2.130$, $g_z = 2.615$.

Estimates of the approximate range of interspin distances consistent with the overall distortion of the CW spectra of the spin-labeled complexes at low temperature were obtained by simulations with the locally-written program MENO.[28] This perturbation calculation includes the effects of anisotropic g values and arbitrary relative orientations of the **g** matrices for the two centers.

Analysis of Saturation Recovery Data for Spin-Labeled Complexes. The relaxation of one type of spin by another type of spin was described by Bloembergen about 40 years ago in an NMR context[29-31] and can be expressed as in eq 1.[32]

$$\frac{1}{T_{1s}} = \frac{1}{T_{1s}^0} + S(S+1)\left[\underbrace{\frac{b^2 T_{2f}}{1+(\omega_f-\omega_s)^2 T_{2f}^2}}_{B\text{ term}} + \underbrace{\frac{c^2 T_{1f}}{1+\omega_s^2 T_{1f}^2}}_{C\text{ term}} + \underbrace{\frac{e^2 T_{2f}}{1+(\omega_f+\omega_s)^2 T_{2f}^2}}_{E\text{ term}}\right] \quad (1)$$

$$b^2 = \frac{8}{3}\left[-\frac{J}{2} - \frac{1}{4} g_s g_f \beta^2 \frac{(1-3\cos^2\theta)}{\hbar r^3}\right]^2$$

$$c^2 = 3 g_s^2 g_f^2 \beta^4 \frac{\sin^2\theta \cos^2\theta}{\hbar^2 r^6}$$

$$e^2 = 3 g_s^2 g_f^2 \beta^4 \frac{\sin^4\theta}{\hbar^2 r^6}$$

where "f" and "s" denote the fast and slow relaxing spins, respectively, T_{1s}^0 is T_1 for the slowly relaxing spin in the absence of spin−spin interaction, T_{1s} is T_1 for the slowly relaxing spin perturbed by the fast relaxing spin, S is the electron spin on the faster relaxing center, ω_f and ω_s are the resonant frequencies for the fast and slow relaxing spins, respectively, r is the interspin distance, J is the electron−electron exchange interaction for the Hamiltonian written as $-JS_1 \cdot S_2$, and θ is the angle between the interspin vector and the external magnetic field.

(24) Quine, R. W.; Eaton, S. S.; Eaton, G. R. *Rev. Sci. Instrum.* **1992**, *63*, 4251.
(25) Quine, R. W.; Eaton, G. R.; Eaton, S. S. *Rev. Sci. Instrum.* **1987**, *58*, 1709.
(26) Salikhov, K. M.; Tsvetkov, Yu. D. In *Time Domain Electron Spin Resonance*; Kevan, L., Schwartz, R. N., Eds.; Wiley: New York, 1979; Chapter 7.
(27) Toy, A. D.; Chaston, S. H. H.; Pilbrow, J. R.; Smith, T. D. *Inorg. Chem.* **1971**, *10*, 2219.
(28) Eaton, S. S.; More, K. M.; Sawant, B. M.; Boymel, P. M.; Eaton, G. R. *J. Magn. Reson.* **1983**, *52*, 435.
(29) Bloembergen, N.; Purcell, E. M.; Pound, R. V. *Phys. Rev.* **1948**, *73*, 679.
(30) Bloembergen, N. *Physica* **1949**, *15*, 386.
(31) Bloembergen, N.; Shapiro, S.; Pershan, P. S.; Artman, J. O. *Phys. Rev.* **1959**, *114*, 445.
(32) Kulikov, A. V.; Likhtenshtein, G. I. *Adv. Mol. Relax. Interact. Processes* **1977**, *10*, 47.

Two modifications of this equation were introduced to adapt it for use in the computer program MENOSR to analyze frozen solution saturation recovery data. (1) $\omega_f - \omega_s$ ($\Delta\omega$) was calculated from the anisotropic g values of the unpaired electrons for each orientation of the molecule with respect to the external field. (2) Equation 1 was originally derived for NMR cases where $\Delta\omega$ is large relative to the spin−spin interaction, which is the first-order or AX approximation. In EPR spectra with overlapping signals, $\Delta\omega$ may be quite small. In the limit where $\Delta\omega$ is small enough that the denominator of the B term goes to 1 eq 1 predicts that the effect on $1/T_{1s}$ is proportional to T_{2f}, which is not reasonable. To exactly describe the contribution to $1/T_{1s}$ as $\Delta\omega$ decreases would require equations comparable to those used in calculations of AB splitting patterns.[28] On the basis of data obtained for the effect of Cu(II) on T_1 of nitroxyl radicals,[33] we propose that a reasonable approximation can be obtained by replacing the B term in eq 1 with eq 2.

$$B \text{ term} = \frac{b^2 T_{2f}}{1 + (\omega_f - \omega_s)^2 T_{2f}^2 + b^2 T_{1f} T_{2f}} \quad (2)$$

The additional term in the denominator of eq 2 is negligible when $\Delta\omega T_{2f}$ is large; however it ensures that in the limit of small $\Delta\omega$ and/or strong interaction (large b), the limiting contribution to $1/T_{1s}$ is $1/T_{1f}$. The physical model is as follows. For cases of relatively weak spin−spin interaction as examined in this paper, the interaction can only enhance the spin−lattice relaxation rate of the slower relaxing center to the extent that it becomes equal to the spin−lattice relaxation rate of the faster relaxing center. This limiting behavior can also be important when the metal T_2 is significantly shorter than the metal T_1.

A random distribution of molecular orientations with respect to the external magnetic field was included. For each of those molecules there is a defined orientation of the interspin vector relative to the axes of the iron **g** matrix. Orientation selection was not included in the calculations. Experimental results suggest that in these complexes orientation selection would be difficult to observe. In the spin-labeled complexes the nitroxyl T_1 showed little variation with position in the EPR spectrum. At X-band, possibilities for orientation selection based on position in the nitroxyl CW spectrum are limited by the orientation dependence of the nitroxyl nitrogen hyperfine splitting (about 30 G). The selectivity is decreased by unresolved proton hyperfine coupling, which contributes about 7 G to the line widths in frozen solution. The interspin distances used in the calculations (10−15 Å) result in maximum dipolar splittings that are of the same order of magnitude as the nitroxyl hyperfine splitting, which largely eliminates possibilities for orientation selection.

Analysis of Spin-Echo Data. Bloembergen's work also predicts an effect of the fast relaxing spin on T_2 for the slower relaxing spin.[29-32] Most of the terms in the expression given in ref 32 for the impact on T_2 are spectral density functions analogous to those in the expression for the impact on T_1 (eq 1). Nitroxyl T_m values between 10 and 150 K are orders of magnitude shorter than T_1. Thus terms that are significant with respect to $1/T_1$ are negligible with respect to $1/T_m$ of the nitroxyl radical. However in the expression for the impact on T_2 there is an additional term, eq 3.[32]

$$\frac{\mu^2 \gamma^2 T_{1f}}{3r^6}(1 - 3\cos^2\theta)^2 \quad (3)$$

where μ is the magnetic moment of the fast relaxing spin, γ is the electron magnetogyric ratio, T_{1f} is T_1 for the fast relaxing spin, θ is the angle between the magnetic field and the interspin vector, and r is the interspin distance. This term reflects the effect on nitroxyl T_2 due to dynamic collapse of the dipolar splitting in the limit where the metal relaxation rate is fast relative to the magnitude of the splitting, i.e. the fast exchange limit.[14] This effect is the dominant effect of the Fe(III) on the nitroxyl ESE data in the temperature regime examined by this report. It can be treated for the full range of metal relaxation rates relative to the spin−spin splittings (both exchange and dipolar) as described in the following paragraph.

Zhidomirov and Salikhov presented the following expression for the impact on the ESE curve of a process that they called "spectral diffusion" in a spin-coupled system.[34]

$$E(2\tau) = R^{-2}\{\exp(-2\tau/\tau_C)[\tau_C^{-2}\sinh^2(R\tau) + R^2\cosh^2(R\tau) + R\tau_C^{-1}\sinh(2R\tau) + \Delta^2\sinh^2(R\tau)]\} \quad (4)$$

where $E(2\tau)$ is the intensity of the echo as a function of τ, τ is the time between microwave pulses in the 2-pulse experiment, τ_C is the correlation time for the dynamic process, Δ is half the angular frequency difference between the two sites averaged by the dynamic process, and $R^2 = \tau_C^{-2} - \Delta^2$. The original expressions[34] used T_{1f} as τ_C. It was subsequently recognized that this expression could be used to analyze the effects on spin-echo decay due to rotation of a methyl group coupled to an unpaired electron.[16] In this case τ_C is the correlation time for the rotation process.

When τ_C is significantly larger or smaller than $|\Delta|$, eq 4 can be simplified.[16] The expressions for the rate constants in these simplified forms are the same as those that are used to obtain approximate rate constants from line widths in dynamic NMR experiments,[14] which makes it clear that the same fundamental principles underlay the interpretation of dynamic NMR line shapes, the collapse of the spin−spin splittings in CW EPR spectra, and the impact of the electron spin relaxation on the ESE data in a spin-coupled system. The limiting forms of eq 4[16] and the regimes in which they were used to improve numerical stability in the program TMDYNAM are given in eqs 5 and 6.

for the slow averaging limit ($1/\tau_C < 0.08|\Delta|$):

$$E(2\tau) = \exp(-2\tau/\tau_C) \quad (5)$$

for the fast averaging limit ($1/\tau_C > 5|\Delta|$):

$$E(2\tau) = \exp[-2\tau(\Delta^2\tau_C/2)] \quad (6)$$

Zhidomirov and Salikhov proposed the use of T_{1f} as τ_C for the spin-coupled pair.[34] In analyzing the spin-echo data in this study it was found that $\tau_C = (T_{1f}T_{2f})^{1/2}$ give better agreement with the experimental data than $\tau_C = T_{1f}$. It was subsequently recognized that in analyzing another problem Wolf showed that for inhomogeneously broadened lines, the statistics can give $\tau_C = (T_{1f}T_{2f})^{1/2}$.[35] For the spin-coupled pair Δ is the orientation-dependent spin−spin splitting, which includes the dipole and exchange contributions. In TMDYNAM Δ is calculated from the expressions that have been used to analyze the spin−spin splitting in CW EPR spectra.[28] The value of Δ was calculated for each orientation of the molecule in the magnetic field.

(33) Eaton, S. S.; Eaton, G. R., unpublished data.

(34) Zhidomirov, G. M.; Salikhov, K. M. *Sov. Phys. JETP* **1969**, *29*, 1037.

(35) Wolf, E. L. *Phys. Rev.* **1966**, *142*, 555.

(36) Du, J.-L.; More, K. M.; Eaton, S. S.; Eaton, G. R. *Isr. J. Chem.* **1992**, *32*, 351.

Depending upon the relative values of $1/\tau_C$ and Δ, eq 4, 5, or 6 was used to calculate the echo decay curve for that orientation. The calculated echo decay curve was multiplied by a single exponential with decay constant T_m to account for other nitroxyl relaxation processes. The powder average decay curve for the frozen solution samples was obtained by summing the contributions from a spherical average of orientations.

The impact of orientation selection was tested in the calculations. The experimental ESE data were recorded at a magnetic field in the center of the nitroxyl spectrum with a microwave B_1 of about 5 G. Only those orientations of the molecule with resonance fields within a specified window around the observing fields were included in the calculated summation. However, so many different orientations of the nitroxyl relative to the external magnetic field contribute to the signal in the center of the spectrum that orientation-selected decay curves (with a window of 5−7 G) agreed within experimental noise levels with curves calculated without orientation selection. A different result could be anticipated in the wings of the spectra, but there the signal to noise was too low to perform the tests.

Selection of Parameters. The parameters in eqs 1, 2, and 4−6 are as follows: r, the distance between the low-spin Fe(III) and the nitroxyl; J, the electron−electron exchange coupling constant; the g values for the two paramagnetic centers; the orientation of the interspin vector relative to the g axes of the low-spin iron; the T_1 and T_2 for the low-spin iron; and the T_1 and T_m for nitroxyl in the absence of the interaction with the Fe(III). Several of these parameters were obtained directly from samples containing only one of the paramagnetic centers. The g values were calculated by simulation of spectra for Fe(TPP)-$(MeIm)_2^+$ and H_2(*trans*-TPP-SL). Nitroxyl T_1 and T_m were obtained from SR and ESE data for H_2(*trans*-TPP-SL). In the absence of interaction with Fe(III) the nitroxyl T_1 is dependent upon position in the spectrum. The values of T_1 at the magnetic field at which the SR data were obtained for the spin-coupled complex were used in the calculations with MENOSR. In the absence of interaction with Fe(III) the nitroxyl T_m is independent of position in the spectrum at the temperatures for which the impact of Fe(III) was examined, which indicates that motional effects that cause orientation-dependent variation of T_m for metal complexes[36] are not significant for nitroxyl radicals in this temperature regime. T_1 and T_2 for low-spin Fe(III) in Fe(TPP)-$(MeIm)_2^+$ between 10 and 28 K were obtained directly by SR or ESE and showed no variation with position in the spectrum, within experimental uncertainty.

The definitions of the angles that relate orientations of the interspin vector and the **g** matrices for the two paramagnetic centers are the same as used in MENO (Figure 1 in ref 28). The angle between the interspin vector and the z axis of the Fe(III) **g** matrix is ϵ and the angle between the projection of the interspin vector and y axis of the Fe(III) **g** matrix is η.[28] The calculated echo decay curves for magnetic fields in the center of the spectrum, with the 5−7 G orientation-selection window or without orientation selection, were weakly dependent upon relative orientations. The angles that were used in the calculations shown below were $\epsilon = 90°$, $\eta = 45°$ for Fe(*trans*-TPP-SL)$(MeIm)_2^+$ and $\epsilon = 60°$, $\eta = 45°$ for Fe(*cis*-TPP-SL)-$(MeIm)_2^+$. These parameters were selected based on the orientations observed in doped single-crystal studies of the Cu(II) complexes of these spin-labeled porphyrins.[37] The same angles were used for the simulations of the SR curves. In orientation-selected calculations of the ESE decays the angle between the z axis of the nitroxyl **g** matrix and the z axis of the Fe(III) **g** matrix is denoted A_1 and the angle between the projection of the nitroxyl z axis on the xy plane of the Fe(III) axes and the Fe(III) x axis is denoted A_2.[28] The calculated curves also were weakly dependent upon these parameters. The values of these angles that were used in the calculations shown below were $A_1 = 20°$ and $A_2 = 30°$. It was not possible to test all combinations of ϵ, η, A_1, and A_2, but checks on random combinations indicated that values of r that give an acceptable match with the experimental data for different combinations of the angles differed by less than 1 Å.

In Cu(*trans*-TPP-SL) $|J|$ is 20−32 G in fluid solution (depending upon solvent and temperature)[38] and 1−30 G for conformations observed in a doped single crystal.[37] For Cu(*satd*-TPP-SL) $|J|$ is 4−25 G in fluid solution.[38] For Cu(cis-TPP-SL) $|J|$ is 0−6 G in fluid solution[38] and 0−10 G in a doped single crystal.[37] For Cu(*p*-TTP-SL) J is less than the nitroxyl line width, which is about 3 G.[39] In the copper(II) porphyrin complexes the unpaired electron is in the $d_{x^2-y^2}$ orbital, which points directly at the porphyrin nitrogens and provides an efficient pathway for electron spin delocalization into the porphyrin ring to which the spin label is attached. In the low-spin Fe(III) complexes the unpaired electron is in d_{xz} which provides a substantially less efficient pathway for spin delocalization. It therefore seems reasonable that values of J would be much smaller for the low-spin iron(III) porphyrin complexes than for Cu(II) complexes with the same porphyrin−nitroxyl linkage. SR and ESE data were analyzed first assuming $J = 0$. Additions of non-zero values of J were tested to determine if fit to the data was improved. If J dominates the spin−spin interaction, Δ (in eqs 4−6) is approximately isotropic and the echo decay approaches a single exponential. If dipolar interaction dominates, Δ is highly anisotropic and the echo decay consists of a distribution of exponential decays. For the low-spin Fe(III) complexes examined here, the "*B*" term in eqs 1 and 2 dominates. A distribution of SR decay constants is observed even when J dominates the spin−spin interaction because of the anisotropy in $\Delta\omega$. However, the width of the distribution is increased by increasing dipolar contributions.

In the ESE decay curves there was a small percentage of the spins with a longer decay time characteristic of nitroxyl that was not interacting with Fe(III) or interacting with Fe(III) with such a short electron-spin−lattice relaxation time that it was fully decoupled from the nitroxyl, as in the oxo dimer. (Between 10 and 70 K the ESE decay rate for nitroxyl in the high-spin monomers, Fe(porphyrin−SL)Cl, is so fast that if a small amount of these species were present in the samples, the contribution to the observed echoes would be difficult to detect.) Signals from species other than the low-spin complexes were observed despite the fact that the complexes had been purified by column chromatography and the preparation of the samples was designed to minimize the concentration of the oxo dimer. The percentage of the nitroxyl that was not interacting with low-spin iron was judged from the tail of the echo decay at long τ values. The percent of non-interacting nitroxyl was between 0 and 4.

Results

CW Spectra. The nitroxyl regions of the CW EPR spectra for two of the spin-labeled low-spin iron porphyrins as a function of temperature are shown in Figures 1 and 2. At temperatures

(37) Damoder, R.; More, K. M.; Eaton, G. R.; Eaton, S. S. *J. Am. Chem. Soc.* **1983**, *105*, 2147.

(38) More, K. M.; Eaton, G. R.; Eaton, S. S. *Can. J. Chem.* **1982**, *60*, 1392.

(39) More, K. M.; Sawant, B. M.; Eaton, G. R.; Eaton, S. S. *Inorg. Chem.* **1981**, *20*, 3354.

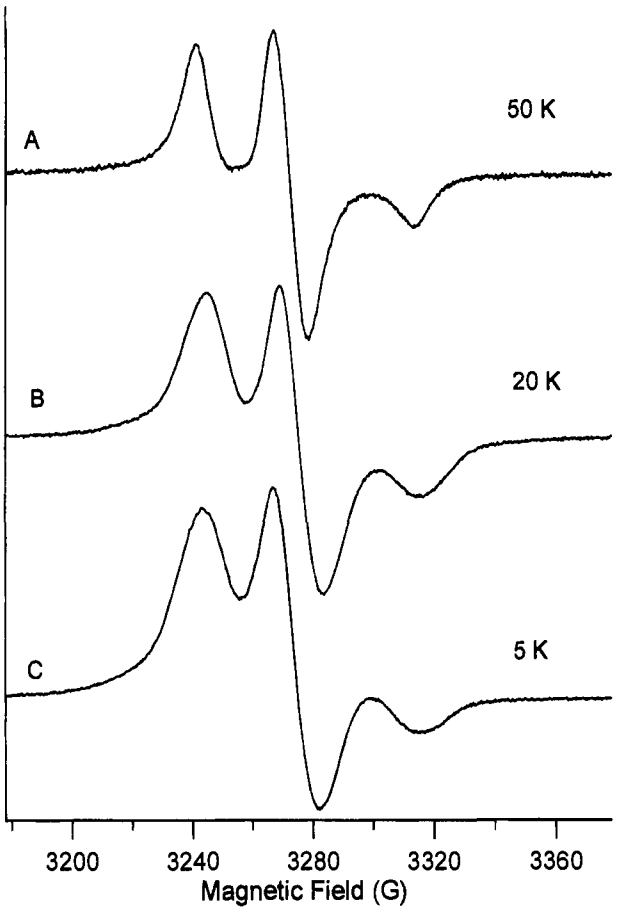

Figure 1. 200 G scans of the nitroxyl portion of the CW EPR spectra of 1 mM low-spin Fe(*trans*-TPP-SL)(MeIm)$_2^+$ in 2:1 toluene−$CHCl_3$ solution containing 10% MeIm at 9.18 GHz. Spectra were obtained with 1.0 G modulation amplitude at 100 kHz, 60 s scan time, and 0.1 s time constant at the following temperatures and microwave powers: (A) 50 K, 0.1 mW, (B) 20 K, 0.05 mW, (C) 5 K, 0.02 mW.

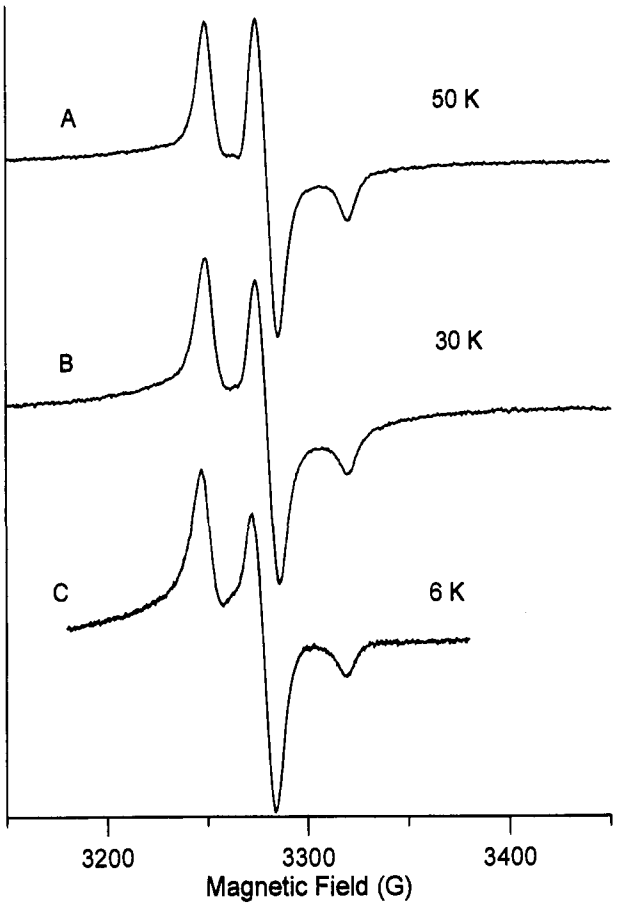

Figure 2. Nitroxyl portion of the CW EPR spectra of 1 mM low-spin Fe(*cis*-TPP-SL)(MeIm)$_2^+$ in 2:1 toluene−$CHCl_3$ solution containing 10% MeIm at 9.18 GHz. Spectra were obtained with 1.0 G modulation amplitude at 100 kHz, 120 s scan time, 0.1 s time constant, and signal averaged for 4 scans at the following temperatures and microwave powers: (A) 50 K, 0.05 mW, (B) 30 K, 0.02 mW, (C) 6 K, 0.8 μW.

above about 50 K the line shapes are typical of immobilized nitroxyls. As the temperature is decreased the line shapes become distorted, but the changes are much smaller than are observed for stronger iron−nitroxyl spin−spin interactions.[9,40] Although the line shape changes with decreasing temperatures are indicative of spin−spin interaction with a faster-relaxing paramagnetic center, the absence of resolved splittings at 5 K precludes a unique simulation. At 5 to 10 K the long electron spin relaxation times for typical organic radicals, including nitroxyl radicals, make it difficult to record spectra that are not broadened by power saturation or distorted by passage effects. Thus careful checks of line shape as a function of microwave power, magnetic field scan rate, and modulation frequency would be needed to ensure the accuracy of these low-temperature line shape changes. At the lowest temperatures in Figure 1 and 2 the spectra did not satisfy slow passage conditions. Use of a lower modulation frequency would have been preferable, but the spectrometer used for these experiments had only 100 kHz modulation. Although uncertainties in line shapes and the lack of resolved features due to spin−spin splitting prevent a unique simulation of the CW spectra, simulations can provide estimates of plausible values of r. These values are summarized in Table 1.

Electron Spin-Echoes. A more direct way to examine the process that results in the temperature dependence of the CW EPR signal is electron spin-echo spectroscopy. In this experiment the echo intensity is recorded as a function of the time between the echo-forming microwave pulses. The time constant for the decay is commonly called the phase memory time, T_m, and includes contributions from all processes that lead to loss of phase coherence of the electron spins. These processes include motion of the molecule as a whole that changes the resonance frequency of a spin,[36] exchange processes such as methyl rotation,[12-16] spin−spin relaxation between the observed spin and matrix electron and/or nuclear spins (T_2), and in the case of interest here the spin relaxation of an electron to which the observed electron is spin-coupled. For a magnetically isolated nitroxyl radical, including H_2(*trans*-TPP-SL), in frozen solution at temperatures below about 60 K, the ESE decay curve

Table 1. Interspin Distances (Å)

complex	CW range[a]	ESE[b]	SR[c]	single crystal of Cu(II) analog[d]
Fe(*cis*-TPP-SL)(MeIm)$_2^+$	9−13	11	10.5	9.2 to 12.5
Fe(*satd*-TPP-SL)(MeIm)$_2^+$	10−14	13	12.5	
Fe(*trans*-TPP-SL)(MeIm)$_2^+$	12−15	14	13	13.0 to 15.5
Fe(*p*-TTP-SL)(MeIm)$_2^+$	13−17	15		

[a] Approximate range of interspin distances for which some orientation of the interspin vector relative to the nitroxyl axes gives qualitative agreement with the CW spectra at low temperature. [b] Value of r obtained by analysis of nitroxyl T_m using eqs 4−6 and the temperature-dependent Fe(III) relaxation rates. Uncertainty ±1 Å. [c] Value of r obtained by analysis of nitroxyl T_1 using eqs 1 and 2 and the temperature-dependent Fe(III) relaxation rates. Uncertainty ±1 Å. [d] Values of r for conformations of the analogous Cu(II) complexes in a doped single crystal; data taken from ref 37.

(40) Fielding, L.; More, K. M.; Eaton, G. R.; Eaton, S. S. *J. Am. Chem. Soc.* **1986**, *108*, 618.

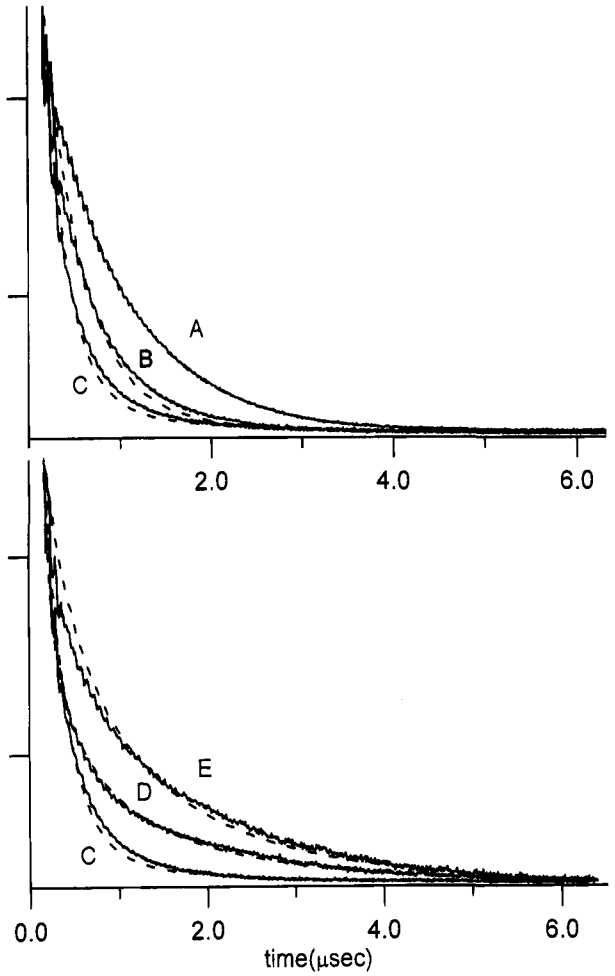

Figure 3. Temperature dependence of ESE decay for Fe(*trans*-TPP-SL)$(MeIm)_2^+$ in 2:1 toluene−$CHCl_3$ solution containing 10% MeIm at 9.18 GHz: (A) 8 K, (B) 22 K, (C) 27 K, (D), 36 K, and (E) 49 K. The data at 27 K are shown in both halves of the figure. The dashed lines were calculated using eqs 3−6 with $r = 14$ Å, $J = 0$, and $\tau_C = (T_1T_2)^{1/2}$ for Fe(III). See discussion in text for additional parameters.

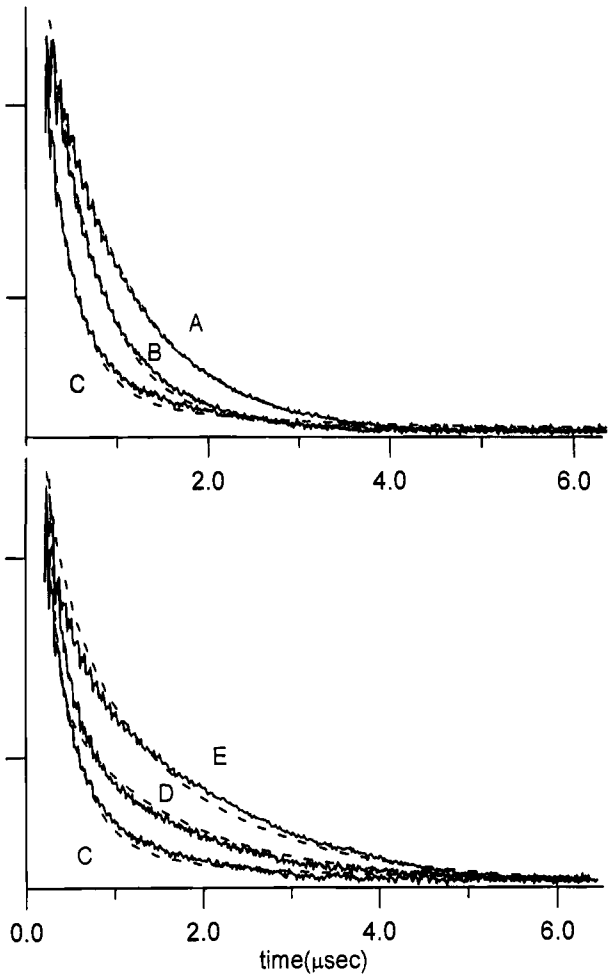

Figure 4. Temperature dependence of ESE decay for Fe(*cis*-TPP-SL)-$(MeIm)_2^+$ in 2:1 toluene−$CHCl_3$ solution containing 10% MeIm at 9.18 GHz: (A) 13 K, (B) 22 K, (C) 27 K, (D), 32 K, and (E) 49 K. The data at 27 K are shown in both halves of the figure. The dashed lines were calculated using eqs 3−6 with $r = 11$ Å, $J = 0$, and $\tau_C = (T_1T_2)^{1/2}$ with values of T_1 and T_2 for Fe(III) as plotted in Figure 5. See discussion in text for additional parameters.

exhibits little temperature dependence and can be fit to a single exponential decay with $T_m = 3$ to 4 μs.[14] This decay is due to matrix nuclei. Above about 60 K the nitroxyl T_m is decreased due to rotation of the methyl groups at rates comparable to the magnitude of the electron−proton couplings.[12−14]

Typical ESE decay curves for Fe(*trans*-TPP-SL)$(MeIm)_2^+$ in 2:1 toluene−$CHCl_3$ containing 10% MeIm as a function of temperature are shown in Figure 3. As the temperature is increased from 8 to 22 and then to 27 K (Figure 3, curves A, B, and C) the echo decay rate increases dramatically. As the temperature is increased to 36 and 49 K, the decay rate decreases (Figure 3, curves D and E). ESE decay curves for Fe(*cis*-TPP-SL)$(MeIm)_2^+$ in 2:1 toluene−$CHCl_3$ containing 10% MeIm as a function of temperature are shown in Figure 4. Analogous to the behavior of the trans isomer, the echo decay rate increased as the temperature was increased from 13 to 27 K (Figure 4, curves A, B, and C) and decreased as the temperature was increased from 27 to 49 K (Figure 4, curves C, D, and E). Similar trends in echo decay rates were observed for Fe(*satd*-TPP-SL)$(MeIm)_2^+$ and Fe(*p*-TTP-SL)$(MeIm)_2^+$, although the shapes of the decay curves as a function of temperature were different for each complex. The temperature dependence of T_m observed for these complexes is typical of systems undergoing a dynamic process.

The temperature interval over which the changes in echo decay rate was observed is also the temperature interval over which the CW spectra (Figures 1 and 2) exhibited line shape changes—both phenomena are due to dynamic averaging of spin-spin splitting as the low-spin Fe(III) relaxation rate increases with increasing temperature.

To quantitatively interpret the changes in nitroxyl T_m due to interaction with the Fe(III), values are needed for the Fe(III) relaxation rates. SR and ESE spectroscopy were used to measure T_1 and T_2, respectively, for the low-spin Fe(III) in Fe-(TPP)$(MeIm)_2^+$ between 10 and 28 K. These data are shown as solid symbols in Figure 5. The solid line in Figure 5 is the least-squares fit to the T_1 data, $\log(1/T_1) = 7.0 \log(T) - 4.0$. The values of T_2 are weakly temperature dependent at low temperatures, but become more temperature dependent as T_1 approaches T_2 (Figure 5). At 119 and 130 K the iron T_2 was estimated by measurement of the temperature-dependent contribution to the line widths of the CW spectra and these values are included in Figure 5. The open symbols in Figure 5 are the values of T_1 and T_2 for the Fe(III) that were used in the calculations to simulate the effect of the Fe(III) on the nitroxyl T_m and T_1 as discussed below.

The temperature dependence of the nitroxyl ESE curves was analyzed using eqs 4−6 with $\tau_C = (T_1T_2)^{1/2}$ for Fe(III). The following procedure was used for each complex. For data between 10 and 30 K the Fe(III) T_1 and T_2 values were estimated by interpolation from the experimental data in Figure 5. Initially

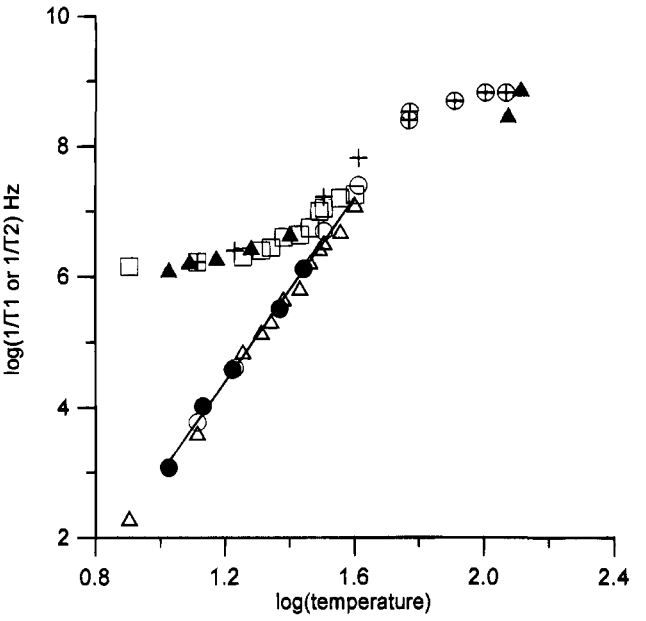

Figure 5. Temperature dependence of electron spin relaxation rates for low-spin Fe(III) in Fe(TPP)(MeIm)$_2^+$: (●) T_1 measured by SR and (▲) T_2 measured by ESE between 10 and 25 K and by temperature-dependent contribution to line width at 119 and 130 K. The solid line is the least-squares fit to the T_1 data: $\log(1/T_1) = 7.0 \log(T) - 4.0$. The open symbols are values obtained by analysis of the effect of the low-spin Fe(III) on relaxation rates for the spin label in Fe(*cis*-TPP-SL)(MeIm)$_2^+$: (△) T_1 and (□) T_2 used in eqs 1 and 2 with $r = 11.0$ Å to analyze nitroxyl T_1, (○) T_1 and (+) T_2 used in eqs 4–6 with $r = 10.5$ Å and $\tau_C = (T_1T_2)^{1/2}$ to analyze nitroxyl T_m.

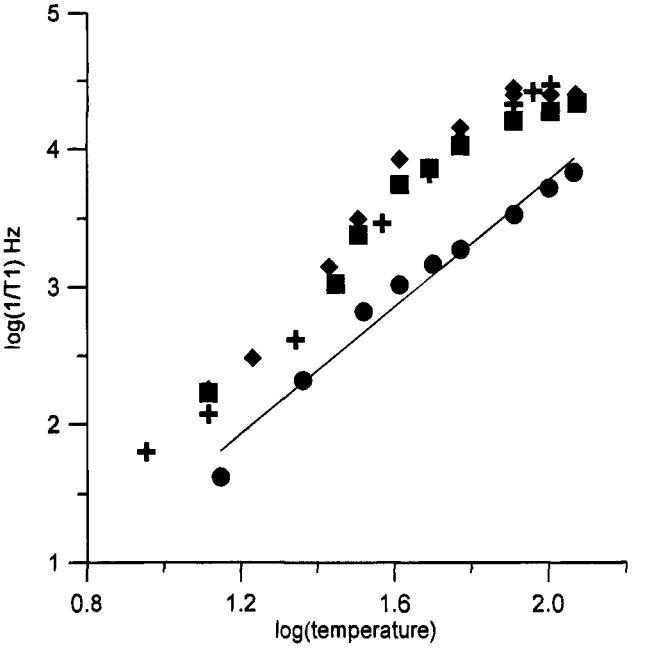

Figure 6. Temperature dependence of nitroxyl T_1 in 2:1 toluene–$CHCl_3$ solution in the absence and presence of low-spin Fe(III) at 9.2 GHz: (●) 1 mM H$_2$(*trans*-TPP-SL), (♦) 1 mM Fe(*cis*-TPP-SL)(MeIm)$_2^+$, (■) 1 mM Fe(*satd*-TPP-SL)(MeIm)$_2^+$, and (+) Fe(*trans*-TPP-SL)(MeIm)$_2^+$. The solid line is the least-squares fit to the data for H$_2$(*trans*-TPP-SL), $\log(1/T_1) = 2.24 \log(T) - 0.677$.

it was assumed that $J = 0$ and r was adjusted to fit the experimental data. The average of the r values from these data sets was then used for all of the data, including data between 10 and 30 K, treating iron T_1 and T_2 as adjustable parameters. Values of iron T_1 above 30 K were extrapolated linearly using the least-squares fit to the data. A smooth curve was used to extrapolate $1/T_2$, intersecting the $1/T_1$ curve at 40 K. These estimated values were then adjusted to fit the experimental data. Since the most likely source of uncertainty in the relaxation rates is uncertainty in sample temperature, T_1 and T_2 were both adjusted following the trends shown in Figure 5. The adjusted values used in fitting the ESE data for Fe(*trans*-TPP-SL)(MeIm)$_2^+$ are shown in Figure 5 (open symbols). Plots similar to Figure 5 were obtained for the other three complexes. Although there is some scatter, it is clear that the values of T_1 and T_2 required to fit the ESE data are within experimental uncertainty of the measured values for the low-spin Fe(III) center between 10 and 28 K. The calculated decay curves are shown as dashed lines in Figures 3 and 4. Both the shapes and the temperature dependence of the ESE decay curves are dependent on r. The values of r that were used to simulate the ESE decay curves are included in Table 1. A change in r by about 0.5 Å caused a detectable deterioration in the agreement between the experimental and calculated data. The shapes of the decay curves also depend upon J. Spin–spin interaction dominated by exchange is inconsistent with the observed decay shapes. The possibility of $J < 1-2$ G cannot be ruled out. However, addition of an exchange contribution did not improve the fit to the data.

Saturation Recovery. Interaction with the rapidly relaxing Fe(III) center decreases the nitroxyl T_1. Values of T_1 obtained by saturation recovery for H$_2$(*trans*-TPP-SL) are shown in Figure 6. The solid line in Figure 6 is the least-squares fit to the data: $\log(1/T_1) = 2.24 \log(T) - 0.677$. This temperature dependence is typical of nitroxyl radicals.[14] For the spin-labeled Fe(III) complexes the SR data for the nitroxyl is a distribution of exponentials due to anisotropy in the low-spin Fe(III) g values and in the spin–spin coupling. The data are not accurately represented by a fit to a single exponential. However, a single-exponential fit provides a qualitative measure of the magnitude of the effect of the Fe(III) on the nitroxyl. The single exponential fits to the nitroxyl data for three spin-labeled complexes are shown in Figure 6, which clearly shows the substantial impact of the Fe(III).

Typical saturation recovery curves for the nitroxyl signal in Fe(*trans*-TPP-SL)(MeIm)$_2^+$ at three temperatures are shown in Figure 7. The SR data were analyzed using eqs 1 and 2, following a procedure analogous to that used for the ESE data. The values of r used to simulate the curves are given in Table 1. The simulated curves are superimposed in Figure 7. Addition of an exchange contribution did not improve the fit to the experimental data. The values of T_1 and T_2 used to simulate the SR curves for Fe(*cis*-TPP-SL)(MeIm)$_2^+$ are included in Figure 5 and are in good agreement with the directly measured values and with the values required to match the ESE data. Since the "B" term in eqs 1 and 2 dominates for these complexes, the calculated nitroxyl SR curves are more sensitive to the iron T_2 than to T_1. However above about 40 K it appears that $T_1 \sim T_2$ (Figure 5).

Discussion

The values of r obtained by ESE and SR (Table 1) agree within experimental uncertainty and fall within the ranges estimated from the CW spectra and observed in the doped single-crystal EPR spectra of the Cu(II) analogs. There probably is some distribution of interspin distances for each complex. The spin–spin splittings (Δ) that are collapsed in the nitroxyl ESE measurements depend on r^{-3} while the perturbation of the nitroxyl SR curves depends on r^{-6}. In a distribution, the stronger dependence on r will weight shorter distances in a distribution more heavily, which may be why the values of r

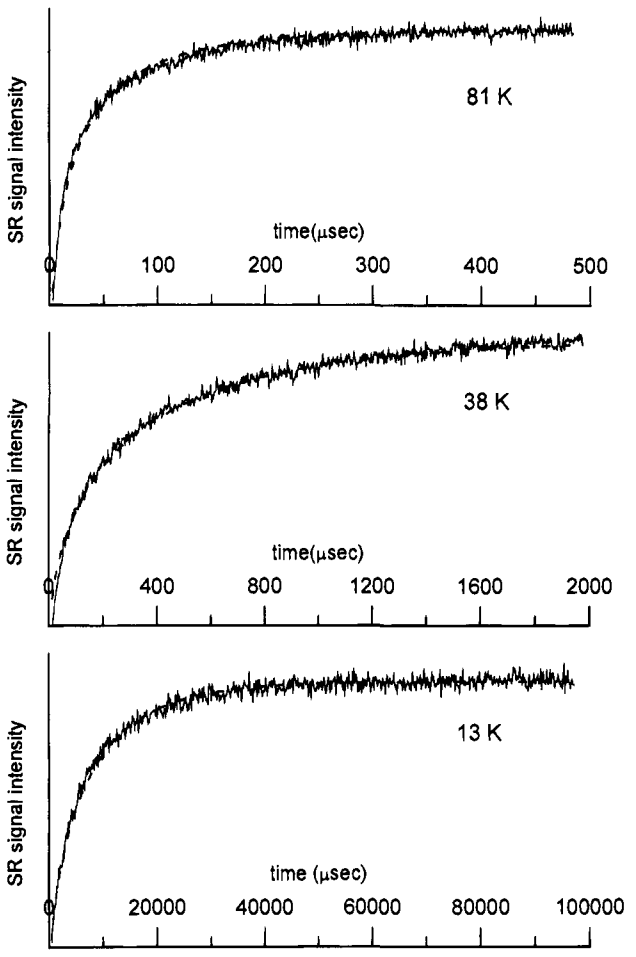

Figure 7. Saturation recovery curves for Fe(*trans*-TPP-SL)$(MeIm)_2^+$ in 2:1 toluene−$CHCl_3$ solution containing 10% MeIm at 9.2 GHz at 13, 38, and 81 K. The dashed lines were calculated with eqs 1 and 2 and r = 13 Å. See text for other parameters.

obtained from the SR data are systematically slightly shorter than the values of r obtained from the ESE data.

This set of complexes was selected for initial study to permit comparison with previous CW studies of the Cu(II) complexes. However, the dipolar interactions at these relatively short distances are large enough relative to the anisotropy of the nitroxyl nitrogen hyperfine that orientation-selected spectroscopy is difficult in frozen solution. For longer interspin distances (and therefore smaller maximum dipolar splittings) it should be possible to examine orientation-selected relaxation data. Since the exchange interaction is isotropic and the dipolar interaction is anisotropic, orientation selected spectra will help to distinguish the two contributions.

The results in this paper demonstrate the power of ESE and SR measurements for the slower relaxing center in a spin-coupled pair combined with direct measurement of relaxation times for the faster relaxing center to determine interspin distances. Previous attempts to use eq 1 to estimate interspin distances have not included measurement of the relaxation rates for the fast relaxing center.[6,7,41,42] Without knowledge of the relaxation rates for the fast relaxing center, the number of unknowns in eq 1 is formidable. To make the problem more tractable, Brudvig and co-workers have used simplified forms of eq 1 and assumed that the distribution in observed relaxation rates for the slowly relaxing center is due exclusively to the anistropy of the dipolar interaction.[41,42] However, a distribution in the relaxation rates for the slowly relaxing center can also arise from other factors including g anisotropy or anisotropy of T_{1f} or T_{2f}. Distributions in T_{1f} and T_{2f}, due for example to a distribution in zero-field splittings, also can contribute to a distribution in relaxation rates for the slower relaxing center. Any of these factors could introduce substantial error in determination of r by the method proposed in refs 41 and 42. It should also be noted that the exchange contribution to eq 1 arises from the same matrix elements (S_1+S_{2-} and S_1-S_{2+}, where 1 and 2 refer to the two interacting centers) as the "B" term. Since J has a sign and the sign of the dipolar interaction changes with orientation, it is important to combine the two contributions before squaring them (as is done in eqs 1 and 2) rather than summing the squares as is done in ref 41.

The analysis of the nitroxyl SR curves provides estimates of the iron relaxation rates at higher temperatures than are accessible by direct measurements. Values of the Fe(III) $T_1 \sim T_2$ estimated at 100−120 K are consistent with estimates based on the temperature-dependent contribution to the CW line shape of $Fe(TPP)(MeIm)_2^+$. Above about 80 K the relaxation rates are less strongly temperature dependent than at lower temperatures. This behavior was observed for the three spin-labeled complexes that were examined.

Stapleton and co-workers[43] examined the temperature dependence of T_1 for low-spin Fe(III) proteins. Between about 5 and 15 K a fit of the data to $1/T_1 = T^n$ gave n = 6.22 to 6.34 for four heme proteins and n = 5.67 for ferredoxin.[43] The values of n were interpreted in terms of the fractal dimensions of the protein.[43] More recently Stapleton concluded, based on studies of copper as well as iron, that "the chain fractal dimension is not simply correlated with relaxation behavior in proteins".[44] The similarity in n for the small-molecule low-spin Fe(III) porphyrin and the low-spin Fe(III) in heme proteins suggests that n is determined more by the local heme environment than by the long-range structure of the protein. The slower change in relaxation rate at higher temperature (Figure 5) is consistent with approach to the high-temperature limit of a Raman process.

Conclusions

Values of T_1 and T_2 for low-spin Fe(III) measured by SR and ESE permit quantitative interpretation of the impact of the rapidly relaxing iron center on the SR and ESE curves for a nitroxyl radical to which it is spin-coupled. The SR and ESE techniques provide consistent values for the interspin distance. Analysis of the nitroxyl SR and ESE data at temperatures where the iron relaxation rates are too fast to measure directly provide information on the Fe(III) relaxation rates. ESE and SR measurements of the signal for the slower-relaxing partner provide information concerning the spin−spin interaction and the relaxation behavior of the faster relaxing partner.

Acknowledgment. The financial support of this work by NIH GM 21156 (G.R.E. and S.S.E.) and NSF CHE8908436 (M.H.R.) is gratefully acknowledged. Dr. Lee Fielding did the initial preparation of Fe(*p*-TTP-SL)Cl in our laboratory.

JA940469S

(41) Hirsch, D. J.; Brudvig, G. W. *J. Phys. Chem.* **1993**, *97*, 13216 and references therein.
(42) Koulougliotis, D.; Innes, J. B.; Brudvig, G. W. *Biochemistry* **1994**, *33*, 11814 and references therein.
(43) Allen, J. P.; Colvin, J. T.; Stinson, D. G.; Flynn, C. P.; Stapleton, H. J. *Biophys. J.* **1982**, *38*, 299.
(44) Drews, A. R.; Thayer, B. D.; Stapleton, H. J.; Wagner, G. C.; Giuliarelli, G.; Cannistraro, S. *Biophys. J.* **1990**, *57*, 157.